https://doi.org/10.1016/j.jsv.2020.115615

Bandgap Formation under Temperature-induced Quasi-periodicity in an Acoustic Duct with Flexible Walls

Yang Liu[a,b], Jingtao Du[a], Li Cheng[b,*],

[a]*College of Power and Energy Engineering, Harbin Engineering University, Harbin, 150001, China*

[b]*Department of Mechanical Engineering, The Hong Kong Polytechnic University, Hong Kong, 999077, China*

*E-mail: li.cheng@polyu.edu.hk

ABSTRACT

This paper is concerned with the acoustic bandgap formation in a duct with periodically flush-mounted flexible walls, subject to a stream-wise temperature variation. A numerical model, based on a piecewise treatment of the arbitrary temperature gradient, is proposed for the accurate prediction of sound propagation in a complex thermal environment. Effects of the system quasi-periodicity due to the temperature change on the bandgap formation, as well as possible mitigation measures through parameter tuning, are revealed. It is shown that, on the top of the resonance bandgap, Bragg reflection bandgap can still be created despite the system quasi-periodicity. In addition to an alteration to the bandgap central frequency due to the temperature-induced acoustic wavelength changes inside the duct, the bandwidths of the bandgaps are also adversely affected, especially when the temperature gradient is large. Numerical analyses show the possibility of tuning and customizing the bandgap formation through a proper selection of the lattice distance and the structural parameters. A combined tuning strategy would warrant a merging of the bandgaps, adjustment of their central frequencies as well as an enlargement of the bandwidth for a given temperature variation range through creating a favorable coupling between the Bragg reflections and the local resonances of the flexible walls.

Keywords: periodic structure; duct acoustics; membrane resonant cell; temperature gradient; bandgaps.

1. Introduction

By analogy with photonic crystals, artificially designed periodic structures have been extensively studied, which offer the potential of tailoring and manipulating acoustic wave propagation [1]. When elastic waves propagate in a periodic elastic medium, bandgaps similar to photonic bandgaps can be generated, leading to the concept of phononic crystals. These structures possess the Bragg-reflection-based bandgap (BBG), within which the acoustic wave propagation is forbidden [2-3], provided the lattice constant is in the same order as the wavelength. Meanwhile, locally resonant structures can also generate bandgap (RBG) with much smaller lattice constant compared to the corresponding wavelength [4]. These phononic crystals may exhibit exotic negative properties such as negative effective bulk modulus [5-8].

The appealing physical properties of periodic structures have also been explored for various acoustic applications such as noise attenuation in ducts. A typical example is the study of periodically arranged Helmholtz resonators (HRs) in a piping/duct system to obtain low frequency bandgaps [5, 9]. In such an arrangement, wave propagation characteristics can be analyzed by the Bloch wave theory and transfer matrix method. The whole system can then be regarded as a homogeneous medium with negative effective properties (mass density or modulus) around the resonant frequency of HRs [10,11]. Besides the HRs, other acoustic devices such as side-branch tubes [12] or micro-perforated tubes [13] have also been studied for the exploration of bandgap features. More relevant to the present work, the use of vibro-acoustic resonant elements on a duct wall has also shown promise for generating effective noise reflection and absorption upon a proper design. For example, replacing a segment of a duct wall by a flexible structure (membrane/plate) would create an effective reflection of the incident acoustic waves towards the upstream of the duct through the vibration of the structure, thus entailing effective sound reduction downstream [14-17]. Subsequently, these vibro-acoustic locally resonant cells have been periodically arranged inside ducts to achieve low frequency resonant/Bragg bandgaps, thus avoiding the drawbacks of conventional duct devices in terms of pressure loss or size limit for low frequency applications [18-20].

More recently, studies on the sound propagation in a duct with temperature variation have attracted increasing research interest due to the frequent occurrence of thermal loading in systems such as gas turbine combustion chambers and exhaust systems [21, 22]. For example, an analytical

solution using an adapted Wentzel-Kramers-Brillouin (WKB) approximation was derived and validated for high frequency noise generation and transmission inside a duct with temperature gradient [23]. A general four-pole matrix based on the continuity, momentum and state equation were established for the general case of standing plane waves in a moving medium with a linear temperature variation [24]. Using suitable transformations, the derived acoustic wave equation can be reduced to solvable Bessel's differential equation for a duct with an arbitrary axial temperature profile [25]. That method was then extended to derive the exact analytical solutions for quadratic [26] and polynomial mean temperature profiles [27]. A unified analytical approach was proposed based on the conservation equations and adapted WKB approximation which allows accurate prediction of the sound propagation with the consideration of arbitrary mean temperature gradient, for both low and moderate-to-high sub-sonic Mach numbers [28]. Meanwhile, studies on the sound attenuation inside duct silencer with temperature gradient have also been reported in the literature. For example, a theoretical prediction scheme was formulated for the four-pole parameters of an expansion chamber in a straight pipe with mean flow and linear temperature gradient [29]. Using similar approach, a quarter-wave tube (QWT) inside a duct with anechoic termination and linear temperature gradient along each duct segment was investigated [30].

Existing studies suggest that moderate temperature variations can sometimes be neglected for the prediction of acoustic performance of mufflers [31], mostly used as stand-alone noise control unit. However, considering the fact that temperature exhibits much significant influence on acoustic wavelength and pressure distribution [28], it is surmised that its effects on periodically arranged noise control units could be different, since the structural periodicity would not perfectly match with the temperature-induced aperiodicity of the acoustic medium inside the duct. In a sense, such a structure can be loosely regarded as quasi-periodic. To the best of our knowledge, the problem of the temperature effect on the bandgap formation inside an acoustic duct has not been fully addressed in the literature, not to mention the exploration of possibilities of exploiting the phenomena to tune the band structure towards a better design of noise control devices.

The above analyses motivated the present research. A theoretical model is proposed for the duct-membrane coupling system in the presence of an ideal temperature distribution. More specifically, a two-fold objective is pursued: a). to propose a numerical model to simulate the acoustic wave propagation inside a duct with flush-mounted periodic flexible membrane units and subject to an arbitrary stream-wise temperature variation and to examine the formation of the bandgap in views

of effective noise attenuation; and b). to explore the possibility of tuning and customizing bandgap properties through a proper tuning of the system parameters. The used temperature field framework and distribution scale were also employed in other literatures [28-30], showing the reasonable assumption and simulation. The rest of the paper is organized as follows. The theoretical formulation on the problem under investigation is first presented. A piecewise treatment of the temperature variation is proposed to allow the handling of arbitrary temperature variation inside the acoustic duct. The proposed modelling approach is then applied to a few benchmark cases and validated through comparisons with existing results and the finite element analyses. In the results and discussion section, Bragg reflection and local resonant bandgap properties are examined under various temperature gradients. Possibilities of customizing bandgap positions as well as their width through adjusting main system parameters, such as the lattice distance and the membrane tension, are discussed under various temperature distributions. Finally, conclusions are drawn.

2. Theoretical formulation

2.1 *Model description*

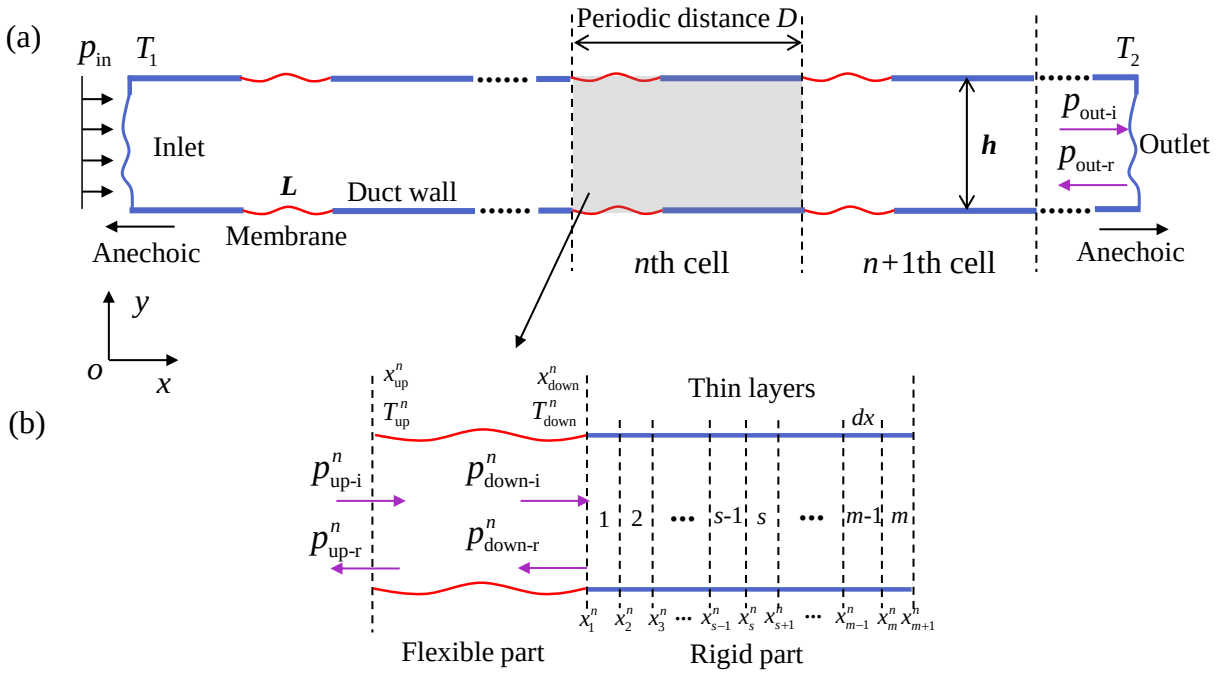

Fig.1. Schematic representation of the model. (a) Duct with periodically arranged flexible walls; (b) the nth unit cell.

Figure 1 illustrates the system under investigation, which consists of a two-dimensional (2-D) duct (height h) with periodically flush-mounted flexible walls (tensioned membranes by default with a length L). p_{in} is the incident sound pressure; and $p_{\text{out-i}}$, $p_{\text{out-r}}$ the sound pressures of the transmitted and reflected sound waves, respectively. The acoustic medium inside the duct bears a temperature gradient $T(x)$ along its length, with inlet and outlet temperatures being denoted as T_1 and T_2, respectively. Actually, arbitrary temperature gradient can be handled in current model, while for simplified analysis, linear distribution function is taken in the followed studies. If one focus on the experimental design, the temperature gradient can be achieved via heating wire with designed twining pattern, and setting proper heating power. A unit cell in the duct is defined as the combination of a membrane and a segment of the rigid duct wall with D denoting the lattice distance between the two adjacent cells. Incident and reflected acoustic waves for each cell can be seen as planar waves when the frequency is lower than the cut-on frequency of the duct. For the nth cell as presented in Fig.1(b), we assume that the temperature over the membrane part is approximated by an averaged temperature $\bar{T}^n = (T^n_{\text{up}} + T^n_{\text{down}})/2$, the validity of which will be verified in the subsequent analyses. Over the rigid portion of the cell, the gas in the duct is sliced into a series of infinitesimally thin gas layers with width dx, each bearing a different constant temperature. As a result, the sound propagation from one layer to the other is accompanied by wave transmission and refection, which govern the wave structure in the duct.

2.2 *Sound propagation in a rigid duct segment with temperature gradient.*

Firstly, considering the sound propagation in the rigid part of the nth cell, which is uniformly meshed along its length with a step size dx=(D-L)/m. The nodes are labelled by x_1^n, x_2^n, …, x_m^n, x_{m+1}^n, with x_1^n and x_{m+1}^n indicating the inlet and outlet of the segment, respectively. In this part, the superscript "n" corresponding to the nth cell will be omitted in the following formulation for simplicity. Crossing from the layer s-1 to s as shown in Fig.1(b), there is a jump in the mean temperature from $T_{s\text{-}1}$ to T_s, thus causing a corresponding jump in both the mean mass density from $\rho_{s\text{-}1}$ to ρ_s and the sound speed from $c_{s\text{-}1}$ to c_s. The pressure and velocity continuity across the cross-section x_s yields

$$p_{\text{i}}^{s\text{-}1} e^{-\text{j}k_{s-1}x_s} + p_{\text{r}}^{s\text{-}1} e^{\text{j}k_{s-1}x_s} = p_{\text{i}}^{s} e^{-\text{j}k_s x_s} + p_{\text{r}}^{s} e^{\text{j}k_s x_s} \tag{1}$$

$$\frac{p_{\text{i}}^{s\text{-}1} e^{-\text{j}k_{s-1}x_s}}{\rho_{s-1}c_{s-1}} - \frac{p_{\text{r}}^{s\text{-}1} e^{\text{j}k_{s-1}x_s}}{\rho_{s-1}c_{s-1}} = \frac{p_{\text{i}}^{s} e^{-\text{j}k_s x_s}}{\rho_s c_s} - \frac{p_{\text{r}}^{s} e^{\text{j}k_s x_s}}{\rho_{s-1}c_s} \tag{2}$$

in which p_i and p_r denote the incident and reflective pressure, j is the imaginary unit and $c=(\gamma R_g T)^{1/2}$, $\rho=p/R_g T$, $k=\omega/c$, γ is the ratio of specific heat, R_g is the universal gas constant and p is the static pressure. Corresponding notations s and s-1 indicate these parameters in different layers. Combining Eq. (1) and (2) gives

$$\begin{bmatrix} p_i^s \\ p_r^s \end{bmatrix} = \begin{bmatrix} \frac{1}{2} e^{jk_s x_s} e^{-jk_{s-1} x_s} \left(1+\frac{\rho_s c_s}{\rho_{s-1} c_{s-1}}\right) & \frac{1}{2} e^{jk_s x_s} e^{jk_{s-1} x_s} \left(1-\frac{\rho_s c_s}{\rho_{s-1} c_{s-1}}\right) \\ \frac{1}{2} e^{-jk_s x_s} e^{-jk_{s-1} x_s} \left(1-\frac{\rho_s c_s}{\rho_{s-1} c_{s-1}}\right) & \frac{1}{2} e^{-jk_s x_s} e^{jk_{s-1} x_s} \left(1+\frac{\rho_s c_s}{\rho_{s-1} c_{s-1}}\right) \end{bmatrix} \begin{bmatrix} p_i^{s-1} \\ p_r^{s-1} \end{bmatrix} = \begin{bmatrix} a_s & b_s \\ c_s & d_s \end{bmatrix} \begin{bmatrix} p_i^{s-1} \\ p_r^{s-1} \end{bmatrix} \tag{3}$$

With the plane wave assumption, Eq. (3), can be transcended to the next layer, as

$$\begin{bmatrix} p_i^{s+1} \\ p_r^{s+1} \end{bmatrix} = \begin{bmatrix} a_{s+1} & b_{s+1} \\ c_{s+1} & d_{s+1} \end{bmatrix} \begin{bmatrix} p_i^s \\ p_r^s \end{bmatrix} \tag{4}$$

The incident and reflected waves in the layer adjacent to the membrane can be expressed as

$$p_i^1 = p_{\text{down-i}} \tag{5}$$

$$p_r^1 = p_{\text{down-r}} \tag{6}$$

Based on Eqs. (3) and (4), a whole set of linear equations in terms of the amplitudes of propagating wave components can be expressed as

$$\begin{bmatrix} a_2 & b_2 & -1 & 0 & \dots & 0 & 0 \\ c_2 & d_2 & 0 & -1 & \dots & 0 & 0 \\ 0 & 0 & a_3 & b_3 & -1 & 0 & \dots \\ 0 & 0 & c_3 & d_3 & 0 & -1 & \dots \\ \dots & \dots & \dots & \dots & \dots & \dots & \dots \\ 0 & 0 & \dots & a_m & b_m & -1 & 0 \\ 0 & 0 & \dots & c_m & d_m & 0 & -1 \end{bmatrix} \begin{bmatrix} p_i^1 \\ p_r^1 \\ p_i^2 \\ p_r^2 \\ \dots \\ p_i^m \\ p_r^m \end{bmatrix} = \begin{bmatrix} 0 \\ 0 \\ 0 \\ 0 \\ 0 \\ \dots \\ 0 \end{bmatrix} = \mathbf{R_n p_n^R} \tag{7}$$

Combining Eqs. (5), (6) and (7), the sound propagation in the rigid part of the nth cell can be characterized with the corresponding transmission matrix denoted by $\mathbf{R_n}$.

2.3 *Modelling of the duct portion with flexible wall*

Consider the sound propagation in the flexible portion of the nth cell as shown in Fig.1(b), ranging from x_{up}^{n} to x_{down}^{n} with an averaged sound speed $\bar{c}=(\gamma \mathrm{R_g}\bar{T})^{1/2}$, wave number $\bar{k}=\omega/\bar{c}$ and density $\bar{\rho}=p\mathrm{R_g}\bar{T}$. Similarly, the superscript "n" denoting the nth cell will also be omitted for simplicity. The pressure amplitude transfer matrix between the two cross-sections of the segment is to be established. The transverse displacement of the flexible membrane with fixed boundaries can be expanded as

$$u(x)=\sum_{q=1}^{S} a_q \sin(q\pi x/L)=\mathbf{\Psi}(x)\mathbf{A} \tag{8}$$

in which S is the truncation number of Fourier series. The membrane vibration is modelled following standard approach [19] and its response is obtained by solving the following standard matrix equation

$$\left(\mathbf{K}-\omega^2\mathbf{M}+\mathrm{j}\omega\mathbf{G}\right)\mathbf{A}=\mathbf{P}_{\mathrm{i\&r}} \tag{9}$$

where $\mathbf{K}$ and $\mathbf{M}$ are the stiffness and mass matrices of the membrane with their items $\{\mathbf{K}\}_{qq'}=qq'\delta_{qq'}F\pi^2/2L$, $\{\mathbf{M}\}_{qq'}=m_s\delta_{qq'}L/2$, in which $\delta_{qq'}$ is Kronecker delta function and the sub-index qq' is used to describe the element position in matrix, taking q, q' =1, 2, 3, …, S. F is the tension force in the membrane and m_s is its mass density. $\mathbf{G}$ is the matrix accounting for the sound radiated by the membrane into the duct, expressed as [19]

$$\{\mathbf{G}\}_{qq'}=\sum_{m_d=0}^{M_d}\frac{\bar{\rho}c_{m_d}(2-\delta_{0m_d})}{2h}\left\{\frac{qq'\pi^2L^2[\cos(q\pi)-e^{-\mathrm{j}k_{m_d}L}][\cos(q\pi)+\cos(q'\pi)]}{(q'^2\pi^2-k_{m_d}^2L^2)(q^2\pi^2-k_{m_d}^2L^2)}-\frac{\mathrm{j}k_{m_d}L^3\delta_{q'q}}{q^2\pi^2-k_{m_d}^2L^2}\right\} \tag{10}$$

where M_d is the series truncation number, and

$$c_{m_d}=\mathrm{j}\bar{c}/\sqrt{\left(m_d\pi/\bar{k}h\right)^2-1} \tag{11}$$

$$k_{m_d}=\omega/c_{m_d} \tag{12}$$

For far filed, plane travelling waves are assumed in this model, while for the near filed around the membrane, cross acoustic modes should be considered. As presented in above equations, m_d is the modal order number of the duct. When m_d is equal to 0, it is then 0 order plane wave; for the case of m_d>1, it will be higher order wave. In Eq. (9), $\mathbf{P}_{\mathrm{i\&r}}$ represents the work done by the incident and reflecting sound waves, which can be expressed as

$$\mathbf{P}_{\mathrm{i\&r}}=p_{\text{up-i}}\vec{\mathbf{P}}_1+p_{\text{down-r}}\vec{\mathbf{P}}_2 \tag{13}$$

in which,

$$\left\{\vec{\mathbf{P}}_1\right\}_q = e^{-\mathrm{j}\bar{k}x_{\mathrm{up}}}\int_0^L \left\{\boldsymbol{\psi}\right\}_q e^{-\mathrm{j}\bar{k}x}dx \tag{14}$$

$$\left\{\vec{\mathbf{P}}_2\right\}_q = e^{\mathrm{j}\bar{k}x_{\mathrm{down}}}\int_0^L \left\{\boldsymbol{\psi}\right\}_q e^{-\mathrm{j}\bar{k}x}dx. \tag{15}$$

Eq. (9) can be rewritten as

$$\mathbf{A} = \left(\mathbf{K} - \omega^2\mathbf{M} + \mathrm{j}\omega\mathbf{G}\right)^{-1}\mathbf{P}_{\mathrm{i\&r}} = \boldsymbol{\Pi}\mathbf{P}_{\mathrm{i\&r}} \tag{16}$$

The inverse matrix $(\mathbf{K}\text{-}\omega^2\mathbf{M}+\mathrm{j}\omega\mathbf{G})^{-1}$ can be written as $\boldsymbol{\Pi}$ for simplification. Based on the continuity of the sound pressure at the cross-sections x_{up} and x_{down}, one has

$$p_{\text{down-i}}e^{-\mathrm{j}\bar{k}x_{\mathrm{down}}} = p_{\text{up-i}}e^{-\mathrm{j}\bar{k}x_{\mathrm{down}}} + p_{\mathrm{rad}}^{+} \tag{17}$$

$$p_{\text{up-r}}e^{\mathrm{j}\bar{k}x_{\mathrm{up}}} = p_{\text{down-r}}e^{\mathrm{j}\bar{k}x_{\mathrm{up}}} + p_{\mathrm{rad}}^{-} \tag{18}$$

in which p_{rad}^{+} and p_{rad}^{-} are the radiated sound pressure by the membrane in x-positive and negative directions, respectively, which can be expressed as

$$P_{\mathrm{rad}}^{+} = e^{-\mathrm{j}\bar{k}L}\frac{\bar{\rho}\bar{c}}{2h}\int_0^L \mathrm{j}\omega u(x')e^{\mathrm{j}\bar{k}x'}dx' = \vec{\mathbf{P}}^{+}\boldsymbol{\Pi}\mathbf{P}_{\mathrm{i\&r}} \tag{19}$$

$$P_{\mathrm{rad}}^{-} = \frac{\bar{\rho}\bar{c}}{2h}\int_0^L \mathrm{j}\omega u(x')e^{-\mathrm{j}\bar{k}x'}dx' = \vec{\mathbf{P}}^{-}\boldsymbol{\Pi}\mathbf{P}_{\mathrm{i\&r}} \tag{20}$$

where

$$\left\{\mathbf{P}^{+}\right\}_q = e^{-\mathrm{j}\bar{k}L}\mathrm{j}\omega\frac{\bar{\rho}\bar{c}}{2h}\int_0^L \left\{\boldsymbol{\psi}\right\}_q e^{\mathrm{j}\bar{k}x}dx \tag{21}$$

$$\left\{\mathbf{P}^{-}\right\}_q = \mathrm{j}\omega\frac{\bar{\rho}\bar{c}}{2h}\int_0^L \left\{\boldsymbol{\psi}\right\}_q e^{-\mathrm{j}\bar{k}x}dx \tag{22}$$

Eqs. (17) and (18) can be rewritten in the following form

$$\begin{bmatrix} p_{\text{down-i}} \\ p_{\text{down-r}} \end{bmatrix} = \begin{bmatrix} \dfrac{Q_1}{e^{-\mathrm{j}\bar{k}x_{\mathrm{down}}}} - \dfrac{\mathbf{P}^{-}\boldsymbol{\Pi}\mathbf{P}_1\mathbf{P}^{+}\boldsymbol{\Pi}\mathbf{P}_2}{Q_2 e^{-\mathrm{j}\bar{k}x_{\mathrm{down}}}} & \dfrac{\mathbf{P}^{+}\boldsymbol{\Pi}\mathbf{P}_2 e^{\mathrm{j}\bar{k}x_{\mathrm{up}}}}{Q_2 e^{-\mathrm{j}\bar{k}x_{\mathrm{down}}}} \\ \dfrac{-\mathbf{P}^{-}\boldsymbol{\Pi}\mathbf{P}_1}{Q_2} & \dfrac{e^{\mathrm{j}\bar{k}x_{\mathrm{up}}}}{Q_2} \end{bmatrix} \begin{bmatrix} p_{\text{up-i}} \\ p_{\text{up-r}} \end{bmatrix} = \mathbf{F}_{\mathbf{n}}\mathbf{p}_{\mathbf{n}}^{\mathbf{F}} \tag{23}$$

where $Q_2 = \mathbf{P}^{-}\boldsymbol{\Pi}\mathbf{P}_2 + e^{\mathrm{j}\bar{k}x_{up}}$, $Q_1 = \mathbf{P}^{+}\boldsymbol{\Pi}\mathbf{P}_1 + e^{-\mathrm{j}\bar{k}x_{down}}$.

Combining Eqs. (5)-(7) and (23), the sound propagation in the nth cell including both the flexible and the rigid portions can be determined by solving these linear equations.

2.4 *Sound attenuation bandgaps prediction*

Consider a duct of L_{d} long, exposed to an arbitrary temperature variation $T(x)(0 \leqslant x \leqslant L_{\mathrm{d}})$ with

N membranes on the duct sidewall. L_f denotes the distance from the duct inlet to the first membrane. Then the mean temperature for the nth membrane can be given by $\bar{T}_n = \{T(L_f + nD - D) + T(L_f + nD + L - D)\}/2$. Considering a plane incident wave at the duct inlet $x = x_{in} = 0$, one has

$$p_{in} = p_0 e^{-jk_{in}x_{in}} \tag{24}$$

In light of Eq. (6), for the cell near the duct outlet, one has

$$p_r^m = p_{out\text{-}r} \tag{25}$$

$$p_i^m = p_{out\text{-}i} \tag{26}$$

The anechoic outlet condition at the extreme end of the duct writes

$$p_{out\text{-}r} = 0 \tag{27}$$

Utilizing the respective sound wave transmission functions for the flexible and rigid portions of the duct (Eqs. (7) and (23)) in conjunction with the boundary conditions (Eqs. (24) and (27)), a series of linear equations for the entire system can be obtained as

$$\begin{bmatrix} p_{in} & 0 & 0 & 0 & 0 & 0 \\ \mathbf{R}_0 & 0 & 0 & 0 & 0 & 0 \\ 0 & \mathbf{F}_1 & 0 & 0 & 0 & 0 \\ 0 & 0 & \mathbf{R}_1 & 0 & 0 & 0 \\ 0 & 0 & 0 & \cdots & 0 & 0 \\ 0 & 0 & 0 & 0 & \mathbf{F}_N & 0 \\ 0 & 0 & 0 & 0 & 0 & \mathbf{R}_N \\ 0 & 0 & 0 & 0 & 0 & p_{out\text{-}r} \end{bmatrix} \begin{bmatrix} \mathbf{p}_0^R \\ \mathbf{p}_1^F \\ \mathbf{p}_1^R \\ \cdots \\ \mathbf{p}_N^F \\ \mathbf{p}_N^R \end{bmatrix} = \begin{bmatrix} p_0 \\ 0 \\ 0 \\ \cdots \\ 0 \\ 0 \end{bmatrix} \tag{28}$$

where $\mathbf{R_0}$ is the transmission function corresponding to the rigid part from duct inlet to the first membrane, and each pair of $\mathbf{F_n}$ and $\mathbf{R_n}$ denotes the transmission matrix of that cell. The out-pressure $p_{out\text{-}i}$ in the duct with periodic membranes and temperature gradient can be determined by solving the above linear equations simultaneously. The insertion loss IL is defined as

$$\mathrm{IL} = 20\log_{10}(\tilde{p}_{out\text{-}i} / p_{out\text{-}i}) = 20\log_{10}(1/\alpha) \tag{29}$$

in which $\tilde{p}_{out\text{-}i}$ is the transmitted sound pressure without flexible membranes and α is the transmitted coefficient. It should be mentioned that, the existence of the temperature variation alters the periodicity of the system within the duct portion occupied by the unit cells. Therefore, a dispersion

analysis, leading to the classically defined bandgaps cannot be carried out for such a quasi-periodic system. As an alternative, the terminology bandgap will be loosely used in the subsequent analyses to designate a frequency band in which significant sound attenuation is observed.

3. Results and discussions

3.1 *Model verification*

A rigid wall duct with a temperature gradient is first used as a benchmark for validating the proposed simulation model. The duct is meshed and divided into thin gas layers, each having its different constant temperature. Consider first a two-layer case, each measuring 0.2 m long with different temperatures, 400 K, ρ_1, c_1(hot) and 298 K, ρ_2, c_2 (cold), with an anechoic outlet. Figs.2(a) and 2(b) show the calculated propagation of a unit incident sound wave at f=800 Hz, from two different directions respectively, alongside the results from finite element (FE) simulations. The COMSOL Multiphysics® modeling software is implemented to obtain the FEA results. In the modelling, Pressure Acoustics and Truss modular are used to simulate the sound field and 1-D membrane structure. Normal Acceleration and Edge Load options are applied to solve the coupling between membrane and duct field. The sound speed and density of the sound filed are defined as the functions of temperature gradient. It can be seen that predicted results agree well with FE simulations. Results indicate that the sound pressure amplitude in the cold segment of the duct is always greater than or equal to the pressure in hot part. Similar comparisons using a three-layer configuration (600 K, 400 K and 298 K), shown in Fig.2(c), also show the generally reducing sound pressure amplitude when entering into the hotter part of the duct. The observed oscillating amplitude is obviously due to the wave reflections at the interfaces separating different temperature zones.

To further validate the proposed model, the configuration used by Morgans [28] is revisited. The case considers a linear mean temperature profile $T(x)=(T_1+(T_2-T_1)x/L_d)$, which is illustrated in Fig.2(d), for which T_1=1600 K is the inlet temperature with a unit incident wave, and T_2=800 K is the outlet temperature with an anechoic boundary condition. Other parameters used in the simulation are: duct length L_d=1 m, universal gas constant R_g=287 $K^{-1}kg^{-1}$, ratio of specific heats γ=1.4, layer size $dx=L_d/100$. When using the present model, 100 layers are used. It can be seen that the predictions from the present model show excellent agreement with both the FEM results and Morgans' solutions. It indicates that when the element is small enough, current piecewise method

is effective to handle the continuous physical process for such duct with temperature gradient field.

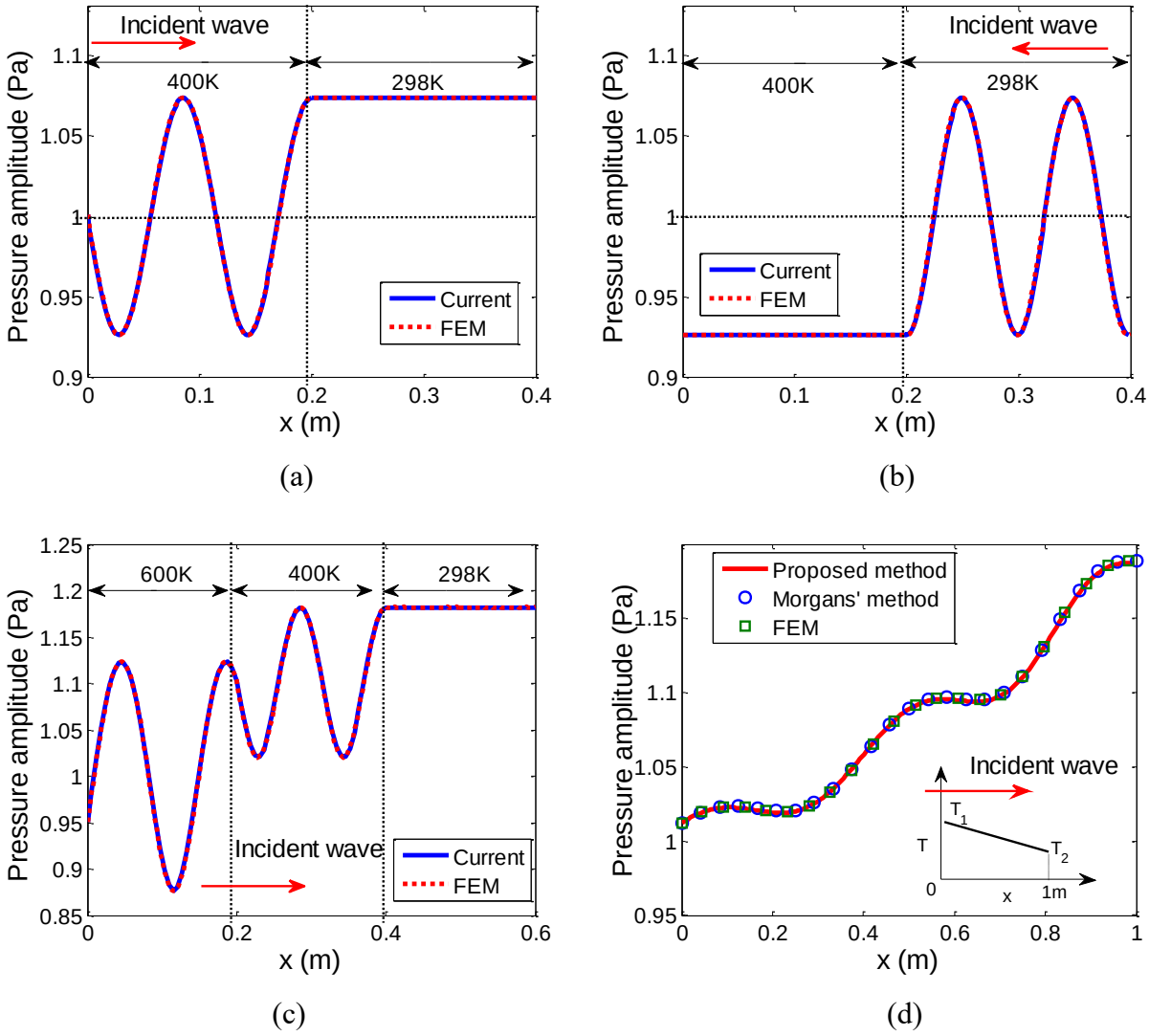

Fig.2. Sound propagation predictions and comparisons with FE results. (a) Two temperature layers, incident wave from hot side. (b) Two temperature layers, incident wave from cold side. (c) Three temperature layers. (d) Linear mean temperature gradient with result from Morgans [28].

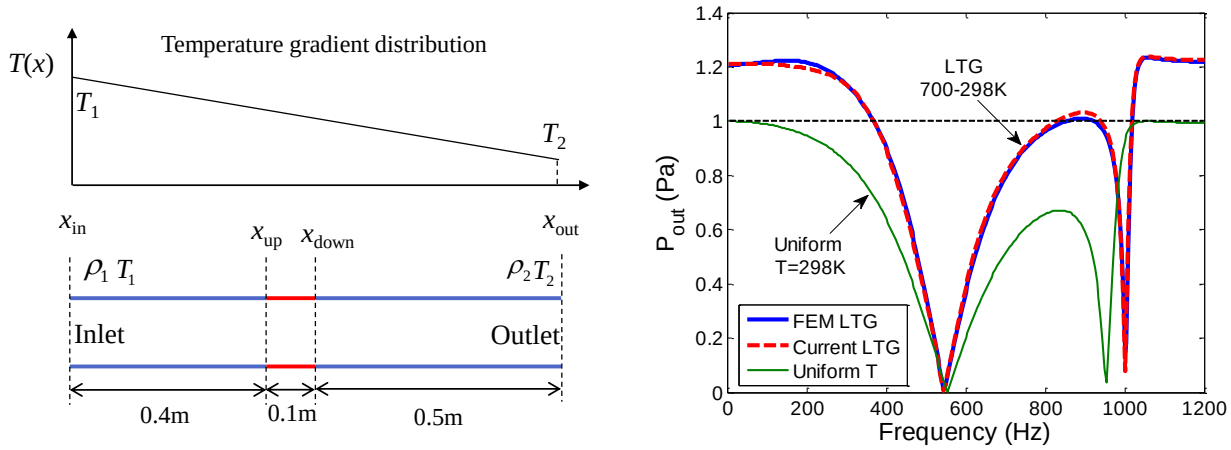

(a) (b)

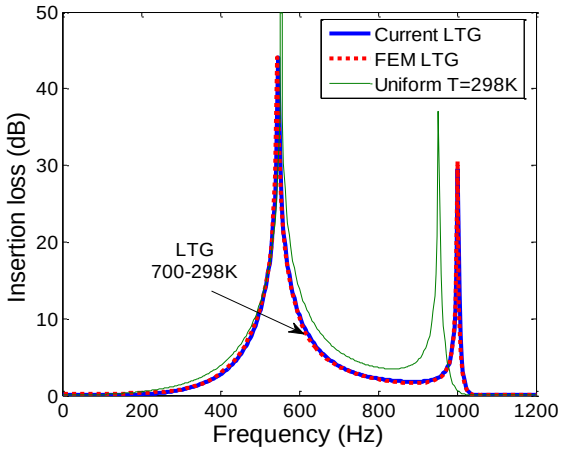

(c)

Fig.3. Sound propagation for the duct-membrane system with a linear temperature gradient (LTG). (a) Schematic representation; (b) Transmission out sound pressure. (c) Insertion loss.

The model is further validated when flexible membranes are included into a duct. The considered case includes a duct of L_d =1 m long, embedded with two segments (one on each side of the duct wall) of tensioned membranes L=0.1 m located at x_{up}=0.4 m, as shown in Fig.3(a). A linear temperature gradient (LTG) with T_1=700 K and T_2=298 K is assumed. In the present model, an averaged constant temperature $\{T(x_{up})+T(x_{down})\}/2$=519 K is taken for the gas over the membrane portion of the duct, while the rigid duct portion is segmented into 100 layers. Other parameters used in the simulation are: duct height h=L, membrane tension force F=1416 N/m and mass surface density 0.12 kg/m^2. Fig.3(b) shows the outlet pressure of the system with a uniform temperature of T=298 K (green solid curve) and LTG (red dashed curve). In the non-resonant region, obvious increase in the sound pressure is observed with LTG. A shift in the resonant peak is also observed due to the changes in the average temperature $\{T(x_{up})+T(x_{down})\}/2$=519 K instead of a constant temperature T=298 K. The insertion loss (IL) is used to evaluate the sound attenuation in Fig. 3(c), along with FE results. It can be seen that they agree very well with each other. The above comparisons validate the established formulation as well as its numerical implementations.

3.2 *Bandgap analyses*

Consider a duct with anechoic boundaries, which comprises five unit-cells with a periodic

distance $D = 0.31$ m. Other membrane parameters remain the same as before. A linear mean temperature profile $T(x)=(T_1+(T_2-T_1)x/L_d)$ is also used in this section with T_1=600 K at the inlet and T_2=298 K at the outlet. The duct length is L_d=0.1 m+5D, where 0.1m is the distance from the duct inlet to the first unit-cell. As mentioned before, the temperature variation results in the quasi-periodicity of the system, thus preventing the use of Bloch wave theory for dispersion analyses. Alternatively, Eq. (6) is solved in conjunction with the transmission function in Eq. (19). Transmitted sound pressure spectra are then used to identify the high sound attenuation (low transmitted sound pressure) bands. Predictions of the transmitted sound pressure at the outlet from the FEM and from the current model are depicted in Fig.4. As a reference, the case with a single membrane is also plotted in the figure. Plateaus, corresponding to low transmitted sound pressure, are loosely referred to as bandgaps here. Obviously, two kinds of bandgaps can be obtained for the five cells case, namely resonant bandgap (RBG) and Bragg reflection bandgap (BBG), as evidenced by the representative acoustic wave distributions, also shown in this figure. At 510 Hz and 1000 Hz in the RBG region, local resonance effects are evidenced by basically the same resonance behavior of the membrane cells. At 810 Hz within the BBG region, however, sound propagates as a plane wave and decreases rapidly along the cells.

Varying the inlet T_1 and keeping the outlet T_2 as a constant, wave propagations for three LTGs, *e.g.* 500-298 K, 600-298 K and 700-298 K, are presented in Fig.5. While only a slight reduction in the bandwidth of the first RBG can be observed as the inlet temperature increases, the BBG is significantly affected. The plausible reason is that an increase in the temperature-induced sound speed $c=(\gamma R_g T)^{1/2}$ would enlarge the acoustic wavelength, thus generating a shift of the BBG to higher frequencies, as shown in Fig.5.

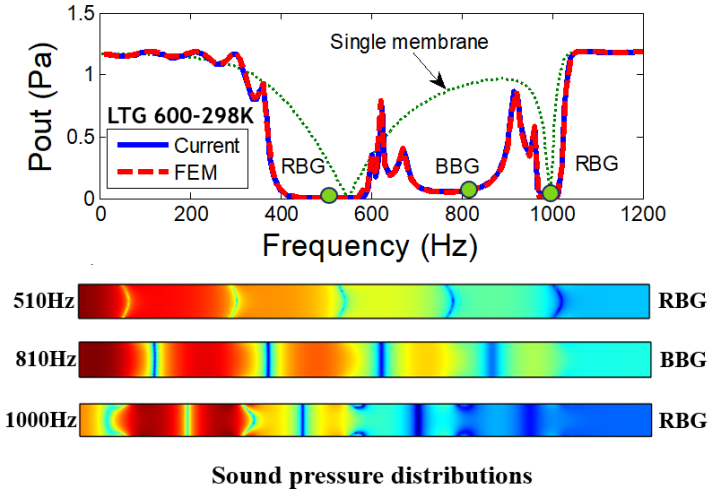

Fig.4. Bandgaps and wave propagation pattern of a duct with five unit-cells with a linear mean temperature gradient.

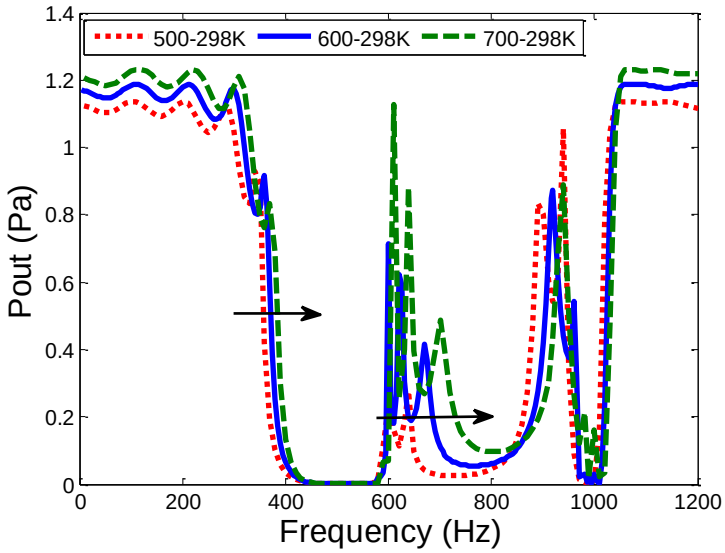

Fig.5. Temperature gradient effect on the bandgap characteristics for three different temperature variations.

To further reveal the effect of the inlet temperature T_1 (by keeping the outlet temperature constant) on the bandgap characteristics, BBG central frequencies are extracted and plotted in Fig.6(a). Two different periodic distances D=0.31 m (red curve) and 0.41 m (blue curve) are examined in the figure. Similarly, a clear shift to high frequency of the Bragg bandgaps in both cases can be observed as T_1 increases. To further illustrate the possible coupling of the BBGs with RBGs, the

first two resonant frequencies of the membrane are marked by the black dashed lines in the figure. It can be seen that, when the central frequency of the BBGs gets closer to one of the local resonant frequencies, exemplified by the three windows denoted by A, B and C, the BBG is coupled with its local resonant counterparts. This also explains the sudden increase in the central frequency of the BBG for the case with D=0.41 m at around 600 K-700 K (Window C in Fig.6(a)). The resulting effect of the bandgap coupling between the BBG and the RBG is shown in Fig.6(b), in which three temperatures, *e.g.* 300 K, 1100 K and 650 K, correspond to windows A, B and C. Meanwhile, corresponding bandwidth variation with the inlet temperature is also depicted in Fig.6(c), in which the red and grey bars denote the BBG and RBG bandwidths, respectively. Black dashed lines denote the approximate location of the central frequencies which are similar to the trend observed in Fig.6(a). It can be seen that, with D=0.31 m, both BBG and RBG shrink and separate apart from each other when the inlet temperature is getting higher. For the case of D=0.41 m, the BBG bandgap is visibly enhanced from 300 K to 500 K, before reaching a strong coupling with the RBG close to 600K up to roughly 900 K. The above analyses suggest that, in addition to the conventional RBGs, the temperature-induced system quasi-periodicity would not completely jeopardize the formation of the BBGs. In addition, results point at the possibility of enlarging the bandwidth of the latter through a proper tuning of the periodic distance to create a favorable coupling with the local resonances of the membranes.

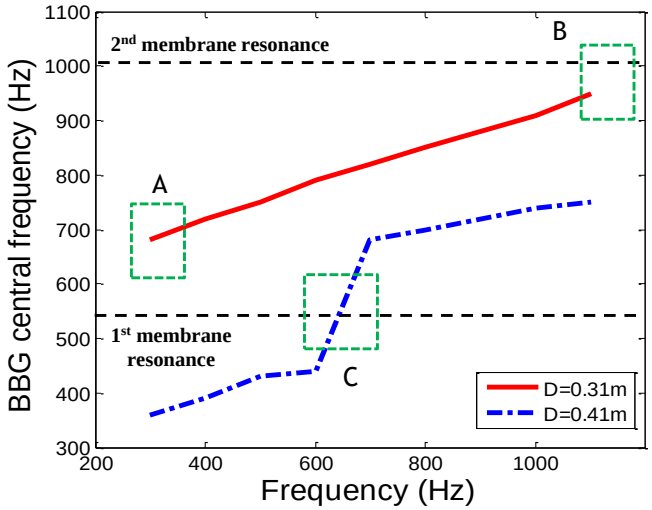

(a)

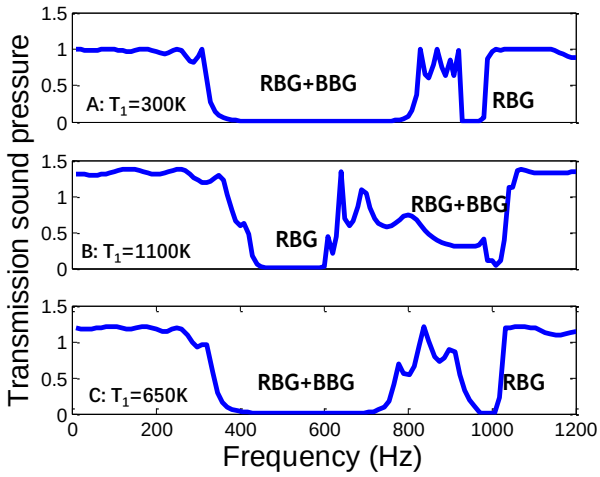

(b)

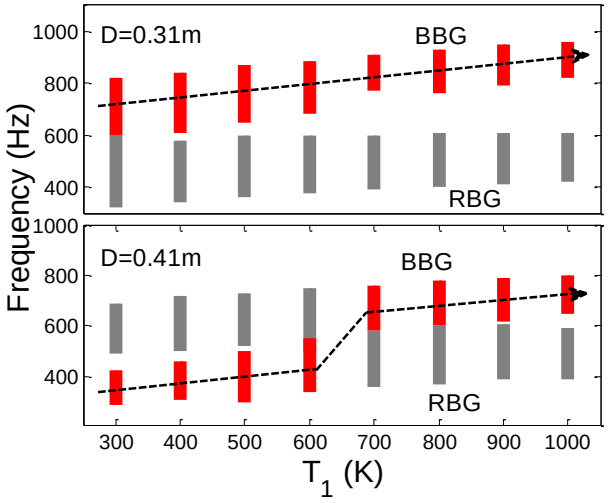

(c)

Fig.6. Bragg reflection and resonant bandgaps analysis. (a) Variation of BBG central frequencies with inlet temperature. (b) Transmission sound pressure for the case of (D=0.31 m, T_1=300K), (D=0.31 m, T_1=1100 K) and (D=0.41 m, T_1=650 K). (c) Bandgap width variation for different T_1.

The idea of possible tuning as well as the achievable benefit are further tested below. Since the temperature gradient alters the periodic characteristics of the acoustic medium and further influence the bandgaps, it is essential to redesign the structural parameters with a due consideration of the thermal effects. As shown in Fig.6(c), changing the cell periodic distance may be an effective way to alleviate the drawback brought by the applied temperature filed. Considering a duct, 2.5 m long and 0.1 m high, carrying a mean axial temperature gradient with a varying inlet temperature T_1 and

a fixed outlet temperature T_2=298 K. The embedded membranes have the same parameters as those used in Fig.3. An optimal lattice length D is given in Fig.7 to create a strong coupling between Bragg reflection and resonant bandgaps, for different inlet temperatures. Taking two representative temperatures at 400 K and 700 K as an example, the corresponding transmitted sound pressure coefficient α are given in sub-figures. It can be seen that the BBG and the 1st RBG are coupled together to generate a much wider bandgap. Taking the optimal lattice length D, the resulting coupled bandgap at different inlet temperatures is also shown in the figure by green bars. It can be seen that although the obtained bandwidth generally decreases when the inlet frequency is getter significantly higher than the outlet temperature (meaning a large temperature gradient inside the duct), the bandgap that can be achieved through the tuning of D is still appreciable.

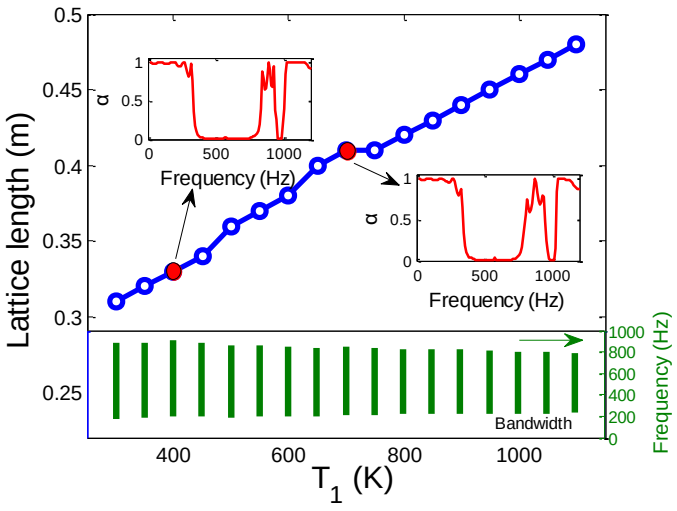

Fig.7. Optimal lattice length D for different inlet temperatures.

Local resonant bandgaps are controlled by the stiffness and the mass of the unit-cells, while the Bragg reflection mainly depends on the spatial lattice distance. Then the frequency of the coupled bandgap (BBG+RBG) can be adjusted via the tuning of the structural stiffness (membrane tension in the present case) and the periodic distance, as demonstrated in our previous work [20], in which a constant temperature field was assumed. The issue is revisited here with a linear temperature gradient. For different inlet temperature T_1 and membrane dimensionless tension $F^*=F/\rho c^2 h$ (ρ and c are the air density and sound speed in uniform temperature T=298 K), optimal periodic distance D can be determined to achieve the strong coupling condition between the BBG and RBG. Four temperature cases with T_1=298 K, 500 K, 800 K, 1100 K, and a constant outlet T_2=298 K are

considered here. The relationship between the optimal distance D and the membrane dimensionless tension F^* is shown in Fig. 8(a). It can be observed that, when the membrane tension decreases, the local resonant bandgap will shift to a lower frequency, thus calling for a corresponding increase in the periodic distance D to cope with this change in order to assure an enlarged BBG. Obviously, if the structure dimension is limited, the applicable range of the membrane tension also reduces for higher temperatures. To provide more details, the central frequency and the bandwidth for T_1=298 K and 800 K are shown in Fig.8(b). It can be observed that the central frequency mainly depends on the membrane tension rather than the applied temperature field. Again, the achievable bandwidth reduces when the temperature distribution inside the duct becomes highly non-uniform (large difference of T_1 and T_2).

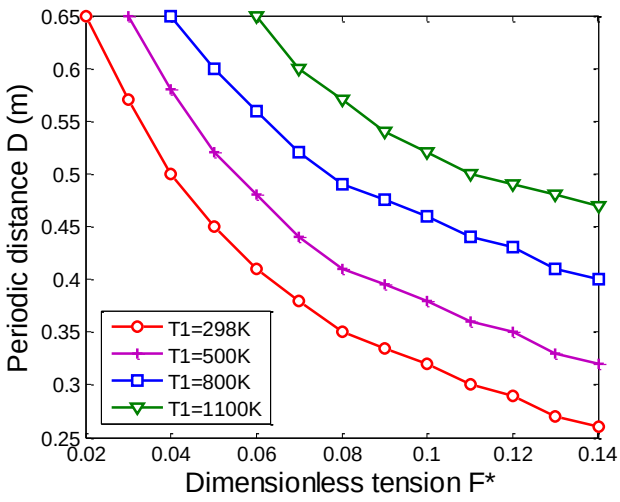

(a)

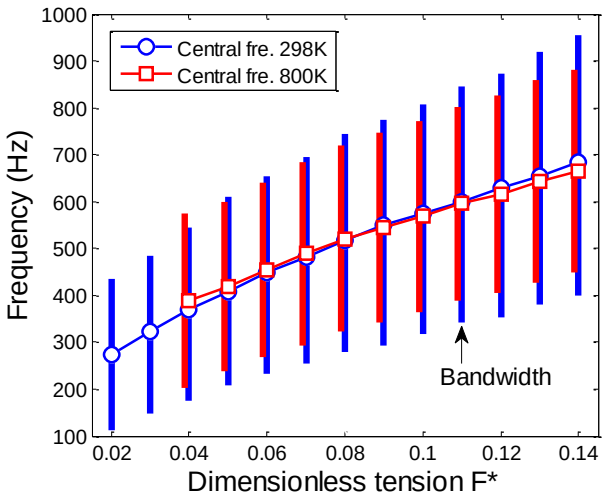

(b)

Fig.8. Coupled bandgap analysis. (a) Matching of membrane tension and periodic distance for different temperatures to create effective coupling. (b) Central frequency and bandwidth of bandgaps for T_1=298 K and 800 K, respectively.

4. Conclusions

Sound propagation inside a duct, with periodically flush-mounted flexible membranes and exposed to a temperature gradient, is studied in this paper. A unified theoretical formulation, capable of dealing with an arbitrary temperature variation, is proposed and validated against finite element results and simulation data reported in the open literature. The model aims at providing a convenient and effective tool for the study and design of duct noise control devices in various temperature environments.

With the embodiment of flexible membrane units on the duct wall, significant sound attenuation bands, loosely referred to as bandgaps, are shown to exist. In addition to the expected resonance bandgaps (RBG), Bragg reflection bandgaps (BBG) can also be created despite the system quasi-periodicity induced by the temperature variations. As the inlet and outlet temperature difference increases, the BBGs are generally shifted to higher frequencies. In general, both BBG and RBG bandwidths are adversely affected when the temperature difference inside the duct becomes larger.

Numerical analyses show the possibility of tuning and customizing the bandgap formation through proper parameter tuning with a due consideration of the temperature effects. In particular, for a given temperature region, a proper tuning of the periodic distance would create favorable coupling between the BBGs and RBGs so that the resulting bandgaps can be greatly enlarged. As such, the drawbacks brought by the applied temperature filed can be alleviated. Further adjusting membrane tension offers additional tunability on the central frequency of the bandgaps. The combined tuning strategy would warrant a merging of the bandgaps, an adjustment of their central frequencies as well as an enlargement of their bandwidths, especially for small temperature differences.

Acknowledgement

This work is supported by the Research Grant Council of the Hong Kong SAR [PolyU 152036/18E], National Natural Science Foundation of China (Grant no. 11972125) and Fok Ying

Tung Education Foundation (Grant no. 161049).

Reference

[1] M.S. Kushwaha, P. Halevi, L. Dobrzynski, B. Djafari-Rouhani, Acoustic band structure of periodic elastic composites, Phys. Rev. Lett.71 (1993) 2022-2025.

[2] M. Sigalas, E.N. Economou, Band structure of elastic waves in two dimensional systems, Solid State Commun. 86 (1993)141-143.

[3] M.M. Sigalas, Defect states of acoustic waves in a two-dimensional lattice of solid cylinders, J. Appl. Phys. 84 (1998) 3026-3030.

[4] Z. Liu, X. Zhang, Y. Mao, Y.Y. Zhu, Z.Y. Yang, C.T. Chan, P. Sheng, Locally resonant sonic materials, Sci. 289 (2000) 1734-1736.

[5] Y.F. Li, H.J. Shen, L.K. Zhang, Y.S. Su, D.L. Yu, Control of low-frequency noise for piping systems via the design of coupled band gap of acoustic metamaterials, Phys. Lett. A 380 (2016) 2322-2328.

[6] M. Yang, G. Ma, Z. Yang, P. Sheng, Coupled membranes with doubly negative mass density and bulk modulus, Phys. Rev. Lett. 110 (2013) 134301.

[7] Z. Yang, J. Mei, M. Yang, N. Chan, P. Sheng, Membrane-type acoustic metamaterial with negative dynamic mass, Phys. Rev. Lett. 101 (2008) 204301.

[8] L. Ning, Y.Z. Wang, Y.S. Wang, Active control of elastic metamaterials consisting of symmetric double Helmholtz resonator cavities, Int. J. Mech. Sci. 153 (2019) 287-298.

[9] X. Wang, C.M. Mak, Wave propagation in a duct with a periodic Helmholtz resonators array, J. Acoust. Soc. Am. 131 (2012)1172-1182.

[10] Z.G. Wang, S.H. Lee, C.K. Kim, C.M. Park, K. Nahm, S.A. Nikitov, Effective medium theory of the one-dimensional resonance phononic crystal, J. Phys.: Condens. Matter 20 (2008) 055209.

[11] S.H. Lee, C.M. Park, Y.M. Seo, Z.G. Wang, C.K. Kim, Acoustic metamaterial with negative modulus, J. Phys. Condens. Matter 21 (2009) 175704.

[12] X.N. Wang, W.Y. Zhu, Y.D. Zhou, Sound transmission in a duct with a side-branch tube array mounted periodically, J. Acoust. Soc. Am. 139 (2016) EL202-EL208.

[13] X.F. Shi, C.M. Mak, Sound attenuation of a periodic array of micro-perforated tube mufflers, Appl. Acoust. 2017 115 (2017) 15-22.

[14] L.X. Huang, Modal analysis of a drumlike silencer, J. Acoust. Soc. Am. 112 (2002) 2014-2025.

[15] X.N. Wang, Y.S. Choy, L. Cheng, Hybrid noise control in a duct using a light micro-perforated plate, J.

Acoust. Soc. Am. 132 (2012) 3778-3787.

[16] Y. Liu, J.T. Du, Coupling effects of boundary restraining stiffness and tension force on sound attenuation of a cavity-backed membrane duct silencer, Appl. Acoust. 117 (2017) 150-159.

[17] M.M. Sucheendran, D.J. Bodony, P.H. Geubelle, Coupled structural-acoustic response of a duct-mounted elastic plate with grazing flow, AIAA J. 52 (2014) 178–194.

[18] M. Farooqui, T. Elnady, W. Akl, Sound attenuation in ducts using locally resonant periodic aluminum patches, J. Acoust. Soc. Am. 139 (2016) 3277-3287.

[19] Y. Liu, J.T. Du, Sound attenuation analysis and optimal design for a duct with periodic membranes embedded in its sidewalls, J. Appl. Phys. 125 (2019) 034901.

[20] Y. Liu, J.T. Du, Acoustic bandgap characteristics of a duct with a cavity-backed and strip mass-attached membrane array mounted periodically, J. Phys. D: Appl. Phys. 52 (2019) 325501.

[21] N. Noiray, M. Bothien, B. Schuermans, Investigation of azimuthal staging concepts in annular gas turbines, Combust. Theor. Model. 15 (2011) 585-606.

[22] D. Laera, K. Prieur, D. Durox, T. Schuller, S.M. Camporeale, S. Candel, Impact of heat release distribution on the spinning modes of an annular combustor with multiple matrix burners, J. Eng. Gas Turb. Power. 139 (2017) 051505.

[23] A. Cummings, Ducts with axial temperature gradients: An approximate solution for sound transmission and generation, J. Sound Vib. 51 (1977) 55-67.

[24] M.L. Munjal, M.G. Prasad, On plane-wave propagation in a uniform pipe in the presence of a mean flow and a temperature gradient, J. Acoust. Soc. Am. 80 (1986) 1501.

[25] R.I. Sujith, G. Waldherr, B. Zinn, An exact solution for one-dimensional acoustic fields in ducts with an axial temperature gradient, J. Sound Vib. 184 (1995) 389-402.

[26] B.M. Kumar, R.I. Sujith, Exact solution for one-dimensional acoustic fields in ducts with a quadratic mean temperature profile, J. Acoust. Soc. Am. 101 (1997) 3798-3799.

[27] B.M. Kumar, R.I. Sujith, Exact solution for one-dimensional acoustic fields in ducts with polynomial mean temperature profiles, J. Vib. Acoust. 120 (1998) 965-969.

[28] J.X. Li, A.S. Morgans, The one-dimensional acoustic field in a duct with arbitrary mean axial temperature gradient and mean flow, J. Sound Vib. 400 (2017) 248-269.

[29] M.G. Prasad, M.J. Crocker, Evaluation of four-pole parameters for a straight pipe with a mean flow and a linear temperature gradient, J. Acoust. Soc. Am. 69 (1981) 916.

[30] C. Howard, Transmission matrix model of a quarter-wave-tube with gas temperature gradients,

Proceedings of Acoustics. 2013.

[31] M.L. Munjal, Acoustics of ducts and mufflers with application to exhaust and ventilation system design, John Wiley & Sons.1987.